An accurate 5D potential energy surface for H$_3$O$^+$–H$_2$ interaction

S. Demes 🆔, F. Lique 🆔, A. Faure 🆔, and C. Rist 🆔

View Online   Export Citation   CrossMark

An accurate 5D potential energy surface for H₃O⁺–H₂ interaction

S. Demes,[1,a]   F. Lique,[1,b]   A. Faure,[2]   and C. Rist[2]

AFFILIATIONS

[1] LOMC, Université du Havre and CNRS, Normandie Université, F-76063 Le Havre, France
[2] Université Grenoble Alpes, CNRS, IPAG, F-38000 Grenoble, France

[a] Author to whom correspondence should be addressed: sandor.demes@univ-lehavre.fr
[b] Electronic mail: francois.lique@univ-lehavre.fr

ABSTRACT

Modeling of the observational spectra of H_3O^+ allows for a detailed understanding of the interstellar oxygen chemistry. While its spectroscopy was intensively studied earlier, our knowledge about the collision of H_3O^+ with the abundant colliders in the interstellar medium is rather limited. In order to treat these collisional excitation processes, it is first necessary to calculate the potential energy surface (PES) of the interacting species. We have computed the five-dimensional rigid-rotor PES of the H_3O^+–H_2 system from the explicitly correlated coupled-cluster theory at the level of singles and doubles with perturbative corrections for triple excitations [CCSD(T)-F12] with the moderate-size augmented correlation-consistent valence triple zeta (aug-cc-pVTZ) basis set. The well depth of the PES is found to be rather large, about 1887.2 cm^{-1}. The *ab initio* potential was fitted over an angular expansion in order to effectively use it in quantum scattering codes. As a first application, we computed dissociation energies for the different nuclear spin isomers of the H_3O^+–H_2 complex.

Published under license by AIP Publishing. https://doi.org/10.1063/5.0015813

I. INTRODUCTION

Hydronium cation H_3O^+ plays a crucial role in oxygen chemistry and ion–molecule reaction schemes, which dominates the chemistry of both dense and diffuse interstellar medium (ISM).[1–9] The recombination of H_3O^+ with electrons as well as its neutralization by charge exchange with a neutral electron donor leads to OH and H_2O formation, where OH can subsequently react with O atoms to form molecular oxygen.[10–13] These ions are also essential probes of cosmic-ray and x-ray ionization rates in diffuse clouds of the ISM.[4,5] These reactive processes then initiate CO production through interactions with interstellar carbon (both neutral and ionized), whereas the build-up of complex polyatomic species in the ISM then follows these basic reactions (for more details, see, for example, the work of Sternberg and Dalgarno[9]). Moreover, the hydronium cation is not just the backbone of oxygen chemistry in the ISM, but it is among the most important cations in chemistry, in general.[14,15]

The vibrational spectroscopy of H_3O^+ and its dissociation dynamics were intensively studied earlier, both experimentally[12,13,15–17] and theoretically.[14,15,18,19] For example, Yu *et al.*[13]

investigated the ground-state inversion transition, rotational constants, and other spectroscopic parameters of hydronium cations in the terahertz frequency region. Mann *et al.*[15] studied the dissociation dynamics of neutral H_3O molecules. In other works,[16,17] the photo-induced fragmentation of hydronium cations was investigated. The dissociative recombination processes of H_3O^+, which have high importance in oxygen chemistry of the ISM, were also intensively studied earlier.[10–12,20]

While the accurate determination of hydronium abundance in astrophysical media requires to model its excitation through radiative and collisional processes, there are only limited works devoted to its collision dynamics. For example, there are no accurate data available in the literature for collisional excitation of hydronium cations by H_2, the most abundant molecule in the ISM. Hence, rate coefficients for rotational excitation of H_3O^+ are missing for interpreting the observations in the ISM. Having the accurate abundance of H_3O^+ can also be used as an indirect method to determine the abundance of interstellar water.[21] The theoretical approaches for bimolecular collision-dynamics calculations require the knowledge of the full intermolecular potential energy surface (PES), which ideally contains all the information about the interaction of the

molecules nuclei and electrons during the collision.[22] The electronic energy and so the whole PES can be computed *ab initio* by solving the electronic Schrödinger equation at fixed nuclear geometries. Once the PES is known, it is possible to infer the probability of the intermolecular reactions as well as the collision cross sections. In order to treat low-energy molecular collisions (e.g., rotational excitation processes), the knowledge of the PES of the ground electronic state is usually enough.

Earlier for modeling the collisions involving hydronium cations, the corresponding data of the isoelectronic NH_3 molecule were used. For example, Offer and van Hemert[3] studied the effect of the inversion motion on the collisional cross sections in rotational excitation of H_3O^+ by H_2 molecules. The collision dynamics of *para-* and *ortho-*H_3O^+ with ground-state *para-*H_2 and *ortho-*H_2 was studied by using the NH_3–H_2 potential. However, such a crude approximation cannot correctly describe the ionic nature of H_3O^+, which is especially important in the long-range part of the interaction potential. In order to improve the model, the authors added a long-range correction to the NH_3–H_2 interaction potential, which was calculated by second-order perturbation theory and fitted by analytical functions.

The electron-impact excitation of H_3O^+ was studied by Faure and Tennyson[23] by combining the **R**-matrix theory with the adiabatic-nuclei-rotation approximation. The rotational excitation of H_3O^+ cations was also studied recently in collision with He atoms, as a template for the H_2 molecule.[21] The authors of this work determined the rotational rate coefficients both for *para-* and *ortho-*H_3O^+ for kinetic temperatures in the range of 5 K–50 K using the close-coupling (CC) approach. They used a 3D PES with fixed intramolecular distances for H_3O^+ (rigid-rotor approximation) in terms of Jacobi coordinates. Their PES was calculated at the level of coupled-cluster theory using single, double, and perturbative corrections for triple excitations [CCSD(T)] along with a non-standard valence quadruple-zeta basis set augmented with bond functions (AVQZ). The *ab initio* interaction potential was calculated for 4788 different geometries with corrections for the basis set superposition error (BSSE), as proposed by Boys and Bernardi.[24] The PES was fitted then by analytical functions in order to implement it in the scattering code. The inversion splitting of the H_3O^+ cation was neglected in their work, which may be valid in the case of NH_3 (the inversion splitting constant is only ~0.8 cm^{-1}[25]) but is questionable for the hydronium ion because of its large inversion constant (~55 cm^{-1}).[13] The global well depth calculated for the H_3O^+–He system is about 354.53 cm^{-1}. The anisotropy of the PES in the work of El Hanini *et al.*[21] was strong at short and intermediate radial distances. It is, however, well established that He is a poor substitute for H_2 in the case of collisional excitation of interstellar ions.[26] Hence, it is crucial and urgent to provide accurate H_3O^+–H_2 collisional data.

The aim of our present work is to introduce a new, highly accurate potential energy surface for the ionic H_3O^+–H_2 collision system. The provided PES will be available to a broad scientific community and can be used for calculating the collisional dynamics of the mentioned system at low energies, i.e., for rotational excitation studies. This paper is organized as follows: In Sec. II, the details of the coordinate system and *ab initio* calculations are discussed along with the fitting procedure of the PES. In Sec. III, we analyze the results obtained for both the potential energy surface and the

bound-states of the complex, while our conclusions and final remarks are presented in Sec. IV.

II. METHODS

A. Coordinate system

We used a Jacobi coordinate system to define the geometry of the H_3O^+–H_2 collision system (see Fig. 1). To reduce the dimensionality, we neglected the intramolecular vibrational motions (rigid-rotor approximation), i.e., the intramolecular O–H and H–H bond lengths as well as H–O–H bond angles were kept fixed during the calculations. We note that the inversion frequency is much larger in H_3O^+ than in NH_3 so that neglecting the tunneling motion of the O nucleus through the plane of the hydrogen nuclei is questionable. Offer and van Hemert[3] have shown, however, that the explicit inclusion of the inversion motion has only a small impact on the rotational cross sections so that the rigid-rotor approximation (vibrational wavefunctions are assumed to be δ-functions, see Ref. 27) is reasonable.

Our intermolecular potential is described then as a function of five inner coordinates: R, θ, ϕ, θ', and ϕ'. These coordinates specify the five dimensions of the PES. The center of the coordinate system (point O in the $Oxyz$ frame) is chosen to be in the center of mass (c.o.m.) of the H_3O^+ cation (molecular frame representation). One of the hydrogen atoms of the H_3O^+ cation (lower left in Fig. 1) is located in the xOz-plane. The R radial parameter defines the O–O' intermolecular distance between the c.o.m. of H_3O^+ (point O) and the c.o.m. of H_2 (point O'). θ and ϕ are spherical angles that characterize the angular position of the c.o.m. of H_2 relative to center O, while the θ' and ϕ' angles define the orientation of the H_2 molecule in the $O'x'y'z'$ coordinate system, which is parallel to $Oxyz$ and its origin is in the c.o.m. of H_2. Similar notations and coordinate systems were used earlier in order to describe the PES for the similar NH_3–H_2[25,28] and H_2O–H_2[29,51] collision systems.

In the case of H_2 molecule, $r_{H-H} = 1.448\,74$ a.u. bond length was employed, which is the average value of the vibrationally ground-state distance of the hydrogen molecule, theoretically calculated without the use of the Born–Oppenheimer approximation.[30] In the case of the H_3O^+ cation, the experimental equilibrium structure was
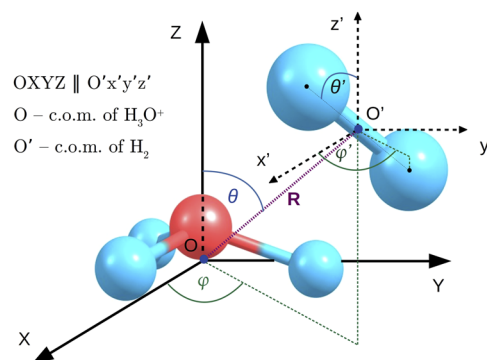

FIG. 1. The coordinate system used to describe the interaction between H_3O^+ and H_2.

used:[31] $r_{\text{O–H}} = 1.8406$ a.u. bond lengths and $\alpha_{\text{H–O–H}} = 113.6°$ bond angles.

B. Electronic structure calculations

All *ab initio* calculations reported in this work were performed using the MOLPRO (version 2015.1)[32,33] and GAUSSIAN (version 09 Rev. E.01)[34] quantum chemistry software packages. At the first step, we performed full geometry optimization in order to find the global minimum of the H_3O^+–H_2 complex. For the first estimations, we applied the regular CCSD theory (without triple corrections) using the augmented correlation-consistent valence triple zeta (aug-cc-pVTZ or AVTZ) basis set with the GAUSSIAN software. After we performed full geometry optimization by the MOLPRO package using the higher-level CCSD(T)-F12 theory with the same basis set to locate the global minimum more precisely. In order to probe the reactivity of the collisional partners, we analyzed the presence or absence of transition states (TSs) between the global minimum of the complex and the dissociated state into H_3O^+ and H_2 products. To locate transition states with a single imaginary vibrational mode, we applied two approaches in the GAUSSIAN code: the Synchronous Transit-Guided Quasi-Newton (STQN) method and the Berny optimization algorithm. In order to further analyze the reactivity, we calculated the enthalpy change of the collision system while modeling the dissociation to different neutral and ionized products. In the low-temperature conditions of the ISM, a chemical reaction has to be exothermic and barrierless in order to proceed, and so the enthalpy change should be negative. The enthalpy of the corresponding species was calculated at 0 K by the explicitly correlated CCSD(T)-F12 method with the AVTZ basis set using the MOLPRO package. The structures of all possible molecular products involved in the reactions were optimized by full geometry optimization at this level of theory. Consequently, the reference structure for enthalpy change calculations was the global minimum geometry of the H_5O^+ complex we found by full geometry optimization (see Fig. 2). After the equilibrium geometries were located, normal mode analysis and thermodynamical properties' calculations were performed to compute the zero-point vibrational energies and the total enthalpy of the products (see below).

In order to choose the most suitable method for large-scale PES calculations, we performed some benchmark computations. First, we searched for the minimum of the rigid-rotor complex. Because
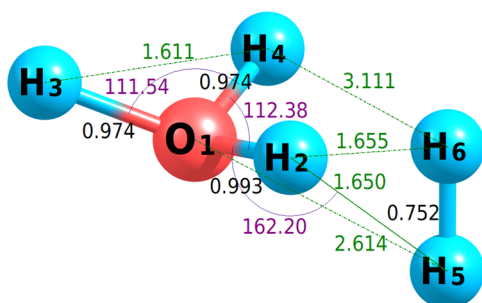

FIG. 2. The global minimum of the non-rigid H_3O^+–H_2 complex. Interatomic distances are in Å, and angles are in degrees.

the constrained geometry optimization is challenging and hard to converge at the explicitly correlated CCSD(T)-F12 level of theory, we used the regular CCSD theory with the AVTZ basis set. During the constrained optimization, we kept the intramolecular H–H and O–H distances fixed at the values discussed in Subsection II A. We found a CCSD/AVTZ rigid-rotor minimum located around $R \simeq 5$ bohrs, $\theta \simeq 102°$, $\phi = 0°$, and $\phi' = \theta' = 90°$ internal coordinates. Based on this geometry, we defined a one-dimensional cut from the overall PES, which connects the origin of the coordinate system with the asymptotic distances and goes through this minimum (θ, ϕ, θ', and ϕ' are fixed, R varies between 3 bohrs and 30 bohrs in the calculations). We will refer to this 1D-cut as a Radial Cut (RC). It is worth noting, however, that this is not the minimum-energy path of the rigid-rotor system. As we found it later from the analytical PES, and as we show in Subsection III B, the coordinates of the global minimum of the rigid-rotor PES slightly differ from the CCSD/AVTZ minimum, typically in angles θ' and ϕ', which define the H_2 orientation. For this reason, throughout this paper, we will not refer to the above-mentioned CCSD/AVTZ minimum anymore.

We evaluated the 1D interaction potential of the H_3O^+–H_2 system along the RC, applying different levels of coupled-cluster theory with double-, triple-, and quadruple-zeta basis sets (AVDZ, AVTZ, and AVQZ, respectively). For the CCSD(T) calculations, the complete basis set (CBS) limit was also calculated for the whole 1D-potential along the RC, based on the three-parameter, mixed Gaussian/exponential method proposed by Peterson *et al.*[35] The comparative analysis of the benchmark calculations (see Fig. 3) has shown that in terms of central processing unit (CPU) time/accuracy for large-scale PES calculations, the best applicable method is the explicitly correlated CCSD(T)-F12 theory combined with a standard AVTZ basis set. As shown in Fig. 3, the well depth of the collision system along the RC is quite large: it is ~1819 cm^{-1} according to the CCSD(T)-F12/AVTZ calculations and ~1840 cm^{-1} according to the results of CCSD(T)/CBS-extrapolation.

The electronic structure of the collision system was tested for possible multiconfigurational factors by analyzing T_1 and D_1 excitation amplitudes in the coupled-cluster calculations. We also evaluated the effects of electronic excitations by calculating the lowest singlet and triplet electronic states of the complex along the RC. For this purpose, the Equation-Of-Motion (EOM)-CCSD and LCC2 response theories were used with the MOLPRO package (for more details, see Refs. 32 and 33 for the software).

To eliminate the effects of the basis set superposition error on the interaction potential, we applied the counterpoise procedure, as proposed by Boys and Bernardi.[24] Hence, our interaction potential is calculated as follows:

$$V(R, \theta, \phi, \theta', \phi') = E_{H_3O^+–H_2} - (E_{H_3O^+} + E_{H_2}), \quad (1)$$

where E denotes the total electronic energy, evaluated in a particular geometry of the whole collision system or its interacting parties. Note that this procedure was applied also for the 1D potentials calculated along the RC (see Fig. 3). Until otherwise noted, we used the following units throughout this paper: atomic units (a.u.) for distances (1 a.u. = 1 bohr $\approx 5.29177 \times 10^{-9}$ cm) and wavenumbers (cm^{-1}) for energies (1 $\text{cm}^{-1} \approx 1/219\,474.624$ hartree).
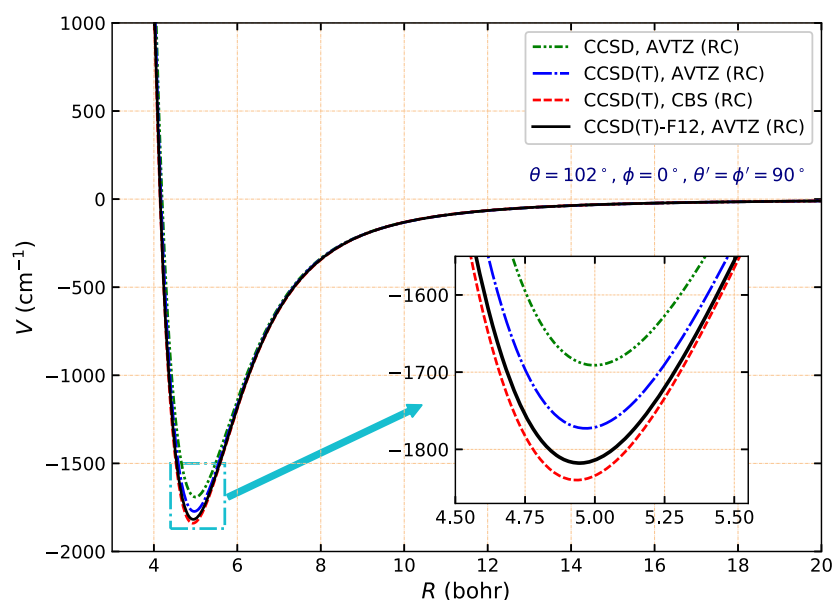
FIG. 3. Comparison of the *ab initio* 1D potentials for the H_3O^+–H_2 system along the RC.

We used a similar formalism to Eq. (1) in order to estimate the interaction energies of the various species within the complex. While performing these calculations, we used only a single geometry—the global minimum of the H_5O^+ complex (the same as the reference geometry for the enthalpy change calculations). It is worth noting that this is not the same geometry that we found for the position of the rigid-rotor minimum. The total energy of the complex and all species was calculated at the CCSD(T)-F12/AVTZ level. The sum in parentheses of Eq. (1) was changed to the sum of total energies of all possible dissociated products whose interaction can lead to the formation of the complex (for details, see Table I). By using this approach, the molecular dissociation is treated as a vertical (Franck–Condon-type) process in which the intramolecular bond lengths and angles are not changing. The calculated interaction energies

are compared with the corresponding reaction enthalpy changes in Table I.

C. PES calculations and fitting

Using Eq. (1) and applying the CCSD(T)-F12/AVTZ method, we calculated the *ab initio* interaction potential for our system, considering 99 000 geometries in total. The R radial distance has been varied between 4 a.u. and 30 a.u. From 4 a.u. to 8 a.u., a step size of 0.25 a.u. was used, and from 8 a.u. to 11 a.u., we increased the step size to 0.5 a.u., while between 11 and 16 a.u., we calculated the potential for every 1.0 a.u. difference. Above 16 a.u. we provided calculations only at the following distances: 18 a.u., 20 a.u., 22 a.u., 25 a.u., and 30 a.u. In order to define the position and the orientation of the

TABLE I. Enthalpy changes and interaction energies for the most relevant reactions involving the H_5O^+ complex. The lowest enthalpy change and absolute interaction energy values are shown in boldface.

	Enthalpy change		Interaction energy	
Reaction process	(eV)	(cm^{-1})	(eV)	(cm^{-1})
$H_5O^+ \rightarrow OH_4 + H^+$	7.225	58 272	−11.396	−91 917
$H_5O^+ \rightarrow OH_4^+ + H$	4.517	36 429	−4.871	−39 292
$H_5O^+ \rightarrow OH_3 + H_2^+$	9.945	80 218	−11.326	−91 355
$H_5O^+ \rightarrow OH_3^+ + H_2$	**0.134**	**1 081**	**−0.243**	**−1 963**
$H_5O^+ \rightarrow OH_3^+ + H + H$	4.598	37 090	−4.995	−40 289
$H_5O^+ \rightarrow OH_2 + H_3^+$	2.892	23 324	−7.651	−61 711
$H_5O^+ \rightarrow OH_2 + H_2 + H^+$	7.213	58 179	−7.747	−62 484
$H_5O^+ \rightarrow OH_2 + H_2^+ + H$	9.030	72 838	−10.517	−84 828
$H_5O^+ \rightarrow OH_2^+ + H_2 + H$	6.200	50 005	−6.759	−54 519
$H_5O^+ \rightarrow OH_2^+ + H_3$	6.529	52 658	−19.274	−155 457
$H_5O^+ \rightarrow OH^+ + H_2 + H_2$	7.204	58 106	−10.256	−82 726

H$_2$ molecule, a set of θ, ϕ, θ', and ϕ' angular parameters was generated via random sampling, leading to 3000 different angular orientations. These parameters were randomized in the following ranges: $0° \leq (\theta, \theta') \leq 180°$ and $0° \leq (\phi, \phi') \leq 360°$. For all particular radial distances R_i, we used the same randomly sampled angular grid.

In order to implement the PES in the HIBRIDON scattering code,[36] the angular expansion must employ a different set of angles for the orientation of the H$_2$ molecule. These angles, denoted by (θ_2, ϕ_2), are defined in Fig. 2 of Ref. 37. In terms of these "body-fixed" coordinates, the intermolecular potential can be expressed as follows:[37]

$$V(R, \theta, \phi, \theta_2, \phi_2) = \sum_{l_1, l_2 = 2m} \sum_{m_1 = 3n \geq 0, m_2} v_{l_1 l_2 m_1 m_2}(R)$$
$$\times \bar{d}_{l_1 l_2 m_1 m_2}(\theta, \phi, \theta_2, \phi_2), \quad (2)$$

where $\bar{d}_{l_1 l_2 m_1 m_2}(\theta, \phi, \theta_2, \phi_2)$ is the normalized basis function,

$$\bar{d}_{l_1 l_2 m_1 m_2}(\theta, \phi, \theta_2, \phi_2)$$
$$= \alpha_{l_1 l_2 m_1 m_2} d^{l_1}_{m_1 m_2}(\theta) d^{l_2}_{m_2 0}(\theta_2) \cos(m_1 \phi + m_2 \phi_2) \quad (3)$$

with the normalization factor

$$\alpha_{l_1 l_2 m_1 m_2} = \frac{1}{2\pi} \frac{1}{(1 + \delta_{m_1 0} \delta_{m_2 0})^{1/2}} \left(\frac{(2l_1 + 1)(2l_2 + 1)}{2} \right)^{1/2}. \quad (4)$$

The functions $d^{l_1}_{m_1 m_2}(\theta)$ and $d^{l_2}_{m_2 0}(\theta_2)$ are the reduced rotation matrices,[37] while the l_1 and l_2 indices refer to the tensor ranks of the angular dependence of the H$_3$O$^+$ and H$_2$ orientation, respectively. It should be noted that symmetry considerations restrict the allowed terms in Eq. (2). Thus, the threefold symmetry of H$_3$O$^+$ requires that m_1 be a multiple of 3. The homonuclear symmetry of H$_2$ similarly constrains l_2 to be even. Full details about symmetry constraints in a symmetric-top and a linear system can be found in Ref. 37.

At each intermolecular distance R, the potential was developed over the angular expansion [Eq. (2)] using a standard linear least-squares fit procedure. We selected a maximum order that includes all anisotropies up to $l_1 = 16$ for H$_3$O$^+$ and $l_2 = 4$ for H$_2$, resulting in 738 $\bar{d}_{l_1 l_2 m_1 m_2}(\theta, \phi, \theta_2, \phi_2)$ functions. All significant terms were selected iteratively using a Monte Carlo error estimator defined in Ref. 38, resulting in a final set of 208 expansion functions with anisotropies up to $l_1 = 16$ and $l_2 = 4$. The root mean square (rms) residual was found to be lower than 1 cm^{-1} in the long-range and minimum region of the interaction potential, i.e., at intermolecular distances $R > 4.75$ bohrs. The mean error on the expansion coefficients $v_{l_1 l_2 m_1 m_2}(R)$ was also found to be smaller than 1 cm^{-1} in this region of the PES. A cubic spline radial interpolation of the coefficients $v_{l_1 l_2 m_1 m_2}(R)$ was finally employed over the whole intermolecular distance range ($R = 4$ bohrs–30 bohrs), and it was smoothly connected to standard extrapolations (exponential and power laws at short- and long-range, respectively) using the switch function defined by Valiron et al.[29] [see their Eq. (10)]. This procedure builds a FORTRAN routine that provides the potential and/or the (continuous) radial expansion coefficients suitable for the bound-state calculations presented below.

D. Bound-state calculations

In order to provide the reference theoretical data for future measurements, we have calculated the lowest rotational bound-state energies of the H$_3$O$^+$–H$_2$ collisional complex. The Hamiltonian for this system can be written as[39]

$$\hat{H} = -\frac{1}{2\mu R} \frac{\partial^2}{\partial R^2} R + \hat{H}_{H_3O^+} + \hat{H}_{H_2} + \frac{\hat{L}^2}{2\mu R^2} + V, \quad (5)$$

where μ is the reduced mass of the system, $\hat{H}_{H_3O^+}$ and $\hat{H}_{H_2}$ are the rotational Hamiltonians of H$_3$O$^+$ and H$_2$, respectively, $\hat{L}$ is the orbital angular momentum of the complex, and V is the interaction potential, as defined by Eq. (2). The umbrella inversion tunneling of the H$_3$O$^+$ monomer was treated with the two-state δ-function model used previously for NH$_3$ complexes (see the Appendix of Ref. 27). Thus, the H$_3$O$^+$ cation is allowed to tunnel between two equilibrium structures, umbrella up and umbrella down, with the inversion angle fixed at the experimental equilibrium value.

The R-dependence of the wavefunctions is expanded in a set of distributed Gaussian functions as a product of stretching and angular functions. The stretching basis functions are composed as

$$\chi_m(R) = \exp\left[-\alpha(R - R_m)^2\right], \quad (6)$$

where α is a scale-factor and R_m is mth value of a uniformly constructed radial grid. The angular basis included all states with total angular momenta $j_{H_3O^+} \leq 18$ for H$_3$O$^+$ as well as $j_{H_2} \leq 3$ and $j_{H_2} \leq 2$ for ortho- and para-H$_2$, respectively. Such a construction method of $\chi_m(R)$ rotational basis functions (which can be used for scattering calculations as well) was proposed by Hamilton and Light.[40] In order to diagonalize the Hamiltonian matrix and to determine the eigenvalues of the bend-stretch states, we used the HIBRIDON scattering code.[36] Calculation of the bend-stretch energies allows one to estimate the D_0 dissociation energies of the complex,

$$D_0 = E_0^{\text{int}} - \varepsilon_j^{\text{ro-vib}}, \quad (7)$$

where E_0^{int} is the internal energy of the ground rotational level of the system in the corresponding nuclear spin configuration and $\varepsilon_j^{\text{ro-vib}}$ is the eigenvalue of the deepest bend-stretch bound state.

We employed the following parameters in the bound-state calculations. In the case of the hydronium cation, we used the most recent experimental rotational constants from Ref. 13: $B = 11.15458$ cm^{-1} and $C = 6.19102$ cm^{-1}. We also considered the 55.34997 cm^{-1} ground-state inversion splitting constant of H$_3$O$^+$ measured by Yu et al.[13] In the case of the H$_2$ molecule, we used $B_{H_2} = 59.3801$ cm^{-1} rotational constant, similarly to the authors of Ref. 25. The reduced mass of the H$_3$O$^+$–H$_2$ system was found to be equal 1.822 49 amu. It is worth noting at this point that we adopted a reduced 55-term expansion of the analytical PES in these benchmark calculations. The PES was not refitted and we simply kept all anisotropies up to $l_1 = 6$, $l_2 = 2$, assuming that the higher-order terms can be neglected for computing the dissociation energies. We tested the quality of this reduced-size PES, and we found that even in the region of the global minimum, its deviation from the full 208-term PES is always within 1%. The bound-state computations were performed by involving both nuclear spin species (ortho- or

o- and *para-* or *p-*) of the collision partners. If we denote the rotational states by j_k^ε, where j is the total angular momentum of the H_3O^+ cation, k is its projection on the C_3 rotational axis, and ε is the (spectroscopic) parity, then for *ortho*-H_3O^+, the quantum number $k = 3n$ (where n = 0, 1, 2, ...), while for *para*-H_3O^+, $k \neq 3n$. We computed the bound-states for all nuclear spin configurations with total angular momenta (J_{tot}) equal 0 and 1, but we could not reach a good convergence in the case of the *para*-H_3O^+–*ortho*-H_2 system for J_{tot} = 1 due to CPU/memory limitations. It is worth mentioning that the ground rotational state of *ortho*-H_3O^+ is the $j_k^\varepsilon = 1_0^+$ state, while in the case of *para*-H_3O^+, that is the $j_k^\varepsilon = 1_1^+$ state. We note that symmetry considerations and the spectroscopic labeling of the bound-states can be found in the work of Surin *et al.*[41] for the similar NH_3–H_2 complex (see Fig. 2 therein). Similar bound-state calculations were performed recently for the NH_3–H_2[41,42] and also for the OH–H_2[39] and NO–H_2[43] collisional systems.

III. RESULTS AND DISCUSSION

A. Structure and reactivity properties of the H_3O^+–H_2 system

The structure of the global minimum of the complex, located by full geometry optimization on the CCSD(T)-F12/AVTZ level of theory, is shown in Fig. 2 along with some interatomic distances and angles. It is worth noting that the interaction energy of the H_3O^+ and H_2 constituents is about −1954 cm^{-1} at this global (nonrigid) minimum. If we compare the intramolecular O–H and H–H bond lengths in this figure with the fixed parameters used in our PES calculations (see Subsection II A for more details), one can see that they only slightly differ from each other. For example, the bond length of the H_2 molecule in the H_5O^+ complex after global optimization is r_{H-H} = 0.752 Å = 1.421 a.u., which is only ~1.5% larger than the experimental equilibrium bond length of the molecular hydrogen (r_{eq} = 1.4 a.u.).[44] Between the bond parameters of H_3O^+ within the fully optimized H_5O^+ complex and the corresponding data of Tang and Oka[31] somewhat larger, but still rather small deviations were observed: up to 1.92% increasing in the O–H bond length and 1.05%–1.8% decreasing in H–O–H bond angles. Thus, as one can see, when a bound complex is formed, the intramolecular bond parameters of the constituent H_3O^+ and H_2 molecules do not change intensively. This states about the chemically non-reactive nature of the H_3O^+–H_2 system. It is worth noting here that the H_3O^+ cation does not preserve its full symmetric-top structure in the global minimum—the closest hydrogen atom is somewhat attracted to the direction of the H_2 molecule (see Fig. 2).

If we examine the intermolecular distances between the atoms of H_2 and those of the hydronium cation in the global minimum of the H_5O^+ complex, one can see the following: The distance between the closest hydrogen atoms is 1.65 Å, while that to the oxygen atom is 2.614 Å. These values are more than two times larger than the corresponding intramolecular distances in the constituent systems: r_{O-H} = 0.974 Å–0.993 Å and r_{H-H} = 0.752 Å (see Fig. 2). According to this, we should consider our collision system not like a covalently bonded, but rather as a van der Waals complex with large intramolecular distances.

As already mentioned earlier in Subsection II B, we probed the possible reaction barriers (transition states) before exploring the

global PES of the interacting system. However, while we applied different search algorithms (STQN and Berny optimization) with several starting geometries and intermolecular orientations, we were not able to locate any TSs in this system. According to our results, the dissociative reactions involving the H_5O^+ van der Waals complex probably proceed without reaction barriers. In order to analyze the barrierless dissociation mechanisms of the system, we calculated the enthalpy change for the possible reactions (for more details, see Subsection II B). The most relevant reactions are shown in Table I. As one can see, all of the possible dissociation channels are endothermic, which enables one to draw the conclusion again that H_5O^+ is a non-reactive complex. The $H_5O^+ \rightarrow OH_3^+ + H_2$ process is characterized with far less enthalpy change than all other reactions. According to this, the most favorable collision path of the complex is toward the formation of H_3O^+–H_2 products. All of the results obtained for the reaction enthalpies are clearly supported by the interaction energies calculated for the same dissociation reactions. The sign "−" here denotes that the H_5O^+ complex is the minimum-energy structure, while its dissociation into different products leads to the increase in total energy.

As shown in Table I, the $H_5O^+ \rightarrow OH_3^+ + H_2$ reaction, which corresponds to the collision process we are interested in, is much more favorable than all other reactions according to the calculated interaction energies. This process is characterized by the smallest energy change compared to the minimum-energy complex, i.e., it is less endothermic than other reactions. We also found that the $OH_3 + H_2^+$ charge exchange reaction is not likely to occur. However, there are some competing reaction channels, which could be significant at higher collision energies, around 20 000 cm^{-1}–40 000 cm^{-1}. Among them, it is worth mentioning the water formation channel $H_5O^+ \rightarrow OH_2 + H_3^+$ as well as the single ($H_5O^+ \rightarrow OH_4^+ + H$) and double ($H_5O^+ \rightarrow OH_3^+ + H + H$) hydrogen loss processes, which are the less endothermic reactions after the $OH_3^+ + H_2$ reaction. The formation of H^+ and H_2^+ cations is even more endothermic and thus less probable. As one can see, all reaction channels except $OH_3^+ + H_2$ can be neglected at the collision energies relevant to the molecular ISM. We note that this is consistent with a reaction rate coefficient lower than 5×10^{-15} cm^3 s^{-1}, as estimated experimentally for the reaction of H_3O^+ with H_2 at 300 K.[45]

The hydrogen (proton) exchange is another relevant process, which could be effective in collisions involving H-containing molecules (ions) and molecular hydrogen. According to Englander *et al.*,[46] the common criteria for hydrogen exchange to proceed are, on one hand, the diffusional collision of the partners to form a hydrogen-bonded encounter complex and, on the other hand, the equilibrium redistribution of the proton between the two members of the hydrogen-bridged complex. As one can see, the intermediate system, which is formed in H_3O^+–H_2 collision, is not a hydrogen-bonded, chemical complex, but rather a van der Waals complex, as mentioned already earlier. According to this, we can neglect the inelastic hydrogen exchange reaction in further calculations and also the *ortho*–*para* symmetry inversion process for H_2 in collisional dynamics studies. Again, this result is consistent with a rate coefficient lower than 10^{-12} cm^3 s^{-1}, as estimated experimentally for the exchange reaction between H_3O^+ and D_2 at 300 K.[47]

In order to analyze the multiconfigurational nature of the H_3O^+–H_2 system, we calculated the lowest electronically excited states along the radial cut, defined in Subsection II B. The two

lowest singlet states (^1A and ^1B) were calculated by different theories: EOM-CCSD and LCC2. The two lowest triplet (^3A and ^3B) states were computed by the LCC2 method. The results of the excited state calculations are shown in Fig. 4. The zero energy value refers to the $^1X(C_1)$ ground state of the system at any particular intermolecular distance R, which was calculated at the same level of theory (EOM-CCSD or LCC2). As one can see, all the lowest excited states are far from the ground state of the system: the closest ^3A is about 9.5 eV–10.7 eV higher than $^1X(C_1)$ at all distances. At the same time, the gap between the calculated excited states is rather small, and they are close to each other everywhere. At some distances, we can observe conical intersections where the excited states cross each other. For example, around $R = 7.5$ bohrs state ^3B crosses the ^3A state, while the singlet ^1A and the triplet ^3B states first meet around 12 bohrs, beyond which they completely coincide. The large gap observed between the ground state and all other electronic states allows us to neglect the excited states in the PES calculations, if the final goal is to study the collision dynamics at energies below a few thousand cm^{-1}.

The last statement is also supported by the results of T_1 and D_1 diagnostics, which were provided in order to give an indication of the quality of results to be expected from the single-reference CCSD(T)-F12/AVTZ calculations along the RC (see the black solid curve in Fig. 3). It is worth noting that the mentioned coupled-cluster method was used for the large-scale PES calculations too. The results of T_1 and D_1 diagnostics for the H_3O^+–H_2 system are shown in the inset graph of Fig. 4. As one can see, the T_1 diagnostic results do not exceed the value of 0.0065, while $D_1 < 0.0133$ at all intermolecular distances. Their mean values are 0.0059 and 0.0108, respectively. The commonly agreed and rather strict indicator of the multi-reference nature of any molecular system is that $T_1 > 0.02$ and $D_1 > 0.05$.[48,49] Our T_1 and D_1 values are much smaller than the suggested critical values, which indicates that our collision complex has a single-reference nature. However, as it was argued also by Lee,[50]
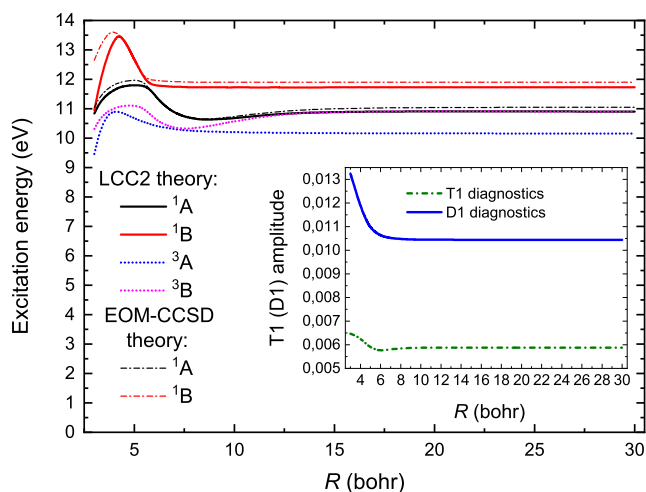
the T_1/D_1 ratio gives an indication of the homogeneity of the electronic structure, and so both diagnostics should be used together with their ratio. According to the author, a perfectly homogeneous electronic structure is characterized by $T_1/D_1 = 1/\sqrt{2}$. The mean value of our T_1/D_1 ratio is about 0.549, which is not equal to $1/\sqrt{2}$ (0.707), but much closer to it compared to the 0.431 mean value obtained by Jiang, DeYonker, and Wilson[49] who derived this value from CCSD/cc-pVTZ results for 148 different molecules, among them H_2O, OH, H_2, NH_3, etc.

B. PES results

The calculated *ab initio* potential was fitted analytically, as described in Subsection II C. Figure 5 shows the comparison of the calculated *ab initio* PES with the results of the fit along some characteristic one-dimensional slices. The first-principles results are indicated by open circles, while the solid lines are constructed analytically from the fit data. In order to understand the choice of the appropriate angular and radial parameters to construct these slices, let us refer to the structural parameters of the RC, which is defined based on $R \simeq 5$ bohrs, $\theta \simeq 102°$, $\phi = 0°$, and $\phi' = \theta' = 90°$ coordinates. It is worth mentioning again that these parameters were found by constrained CCSD/AVTZ optimization and are not coincident with the global minimum of the rigid-rotor PES calculated at the CCSD(T)-F12/AVTZ level.

The fit results are in a good agreement with the reference CCSD(T)-F12/AVTZ potential along the RC, as shown in Fig. 5(a). Some deviations can be observed at small intermolecular distances (below 4 a.u.) where the potential is mainly repulsive. As one can see, the fit around the minimum (near 5 a.u.) somewhat overestimates the *ab initio* results, but both here and in the long-range part of the potential, the analytical potential coincides with the first-principles data within the rms residual. In Fig. 5(b), we tested the angular behavior of the analytical potential. We show 1D potentials as a function of θ spherical angle at different ϕ values. The R radial parameter was kept fixed at 5 a.u., while the two additional angles, which define the orientation of the hydrogen molecule, were also fixed ($\phi' = \theta' = 90°$). As one can see, the quality of the fit in terms of the angular parameters is very good compared to the CCSD(T)-F12/AVTZ results, even when the anisotropy of the potential is rather strong (the value of the potential strongly depends on both spherical angles). We observed only tiny differences in the region of the potential well, i.e., for $\theta = 90°$–$110°$ and only for lower ϕ angles (up to 15°), but these deviations only slightly affect the overall precision of the PES. According to the comparative analysis, the quality of the fit is good enough to use it down to low collision energies.

It is worth noting that while analyzing the results of the fit, we observed larger interaction energies, as compared to the minimum along the RC. For this reason, we provided further iterative calculations to locate the global minimum on the fitted potential energy surface precisely. First, we applied a coarse grid to locate its approximate position, which was then gradually improved. Finally, we could find the coordinates of the global minimum on the analytical PES with a fine grid. The potential is about -1887.2 cm^{-1} at this point, which has the following coordinates: $R \simeq 4.9207$ bohrs, $\theta \simeq 101.362°$, $\phi = 0.000°$, $\theta' \simeq 169.724°$, and $\phi' = 180.000°$. Until otherwise noted, we will refer to these values while talking about

FIG. 4. The lowest electronic excited states of the H_3O^+–H_2 system along the RC. The inset graph shows the T_1 and D_1 diagnostics for the CCSD(T)-F12/AVTZ calculations.
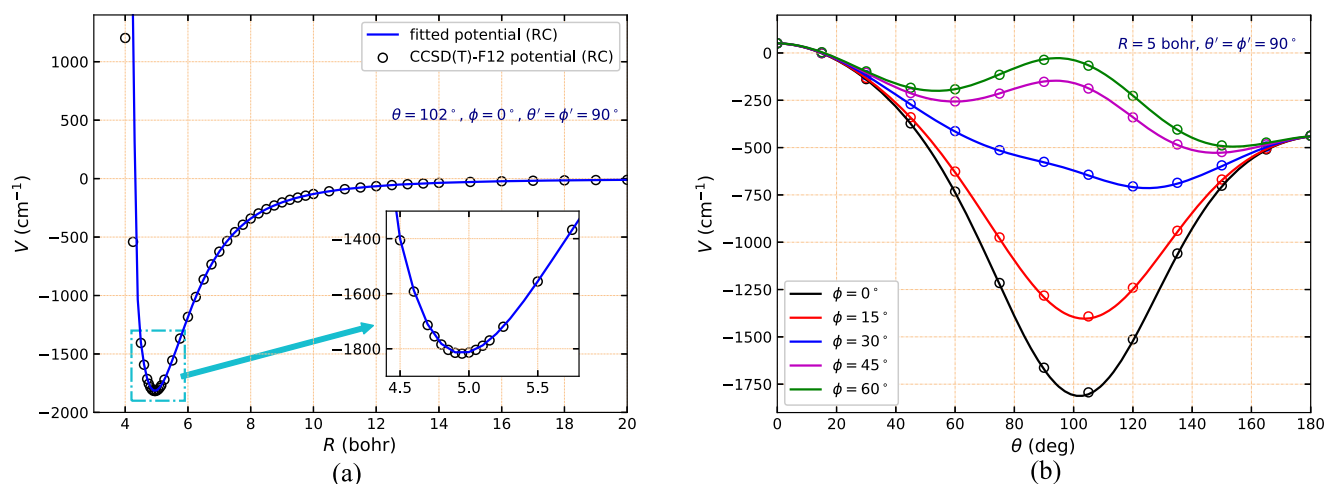
FIG. 5. Comparison of the CCSD(T)-F12/AVTZ potential with the results of the analytical fit. The open circles are for the *ab initio* data, the solid lines are for the fit results. (a) 1D potential: R-dependence along the RC. (b) 1D potential: θ-dependence at different ϕ angles.

the global well depth of the PES and about its coordinates. As one can see, the position of the rigid-rotor global minimum somewhat differs from the coordinates, calculated by the CCSD constrained optimization for the system (see Subsection II B). It is worth noting, however, that larger differences were found only for θ' and ϕ' parameters, which define the orientation of the H_2 molecule. In order to check the quality of the fit at the rigid-rotor minimum, we calculated the interaction potential at the same coordinates on the CCSD(T)-F12/AVTZ level. The *ab initio* result we got for the potential here is about -1889.6 cm^{-1}, which only slightly differs from the value we found based on the analytical fit. The resulting difference is also close to the rms residual of the fit, which is about 0.7 cm^{-1} at $R = 5$ bohrs and 1.4 cm^{-1} at $R = 4.75$ bohrs.

In order to estimate the general anisotropy of the PES, we also analyzed its dependence from the different angular parameters and the radial distance. The results are shown in the contour plots [Figs. 6(a)–6(g)]. Each contour plot visualizes a slice of the PES depending on two parameters, which are indicated by the axis labels. Since our coordinate system is defined by five parameters, it is obvious that every contour plot was constructed by keeping the three additional coordinates fixed. The fixed coordinates for the contour plots were chosen based on the radial cut defined in Subsection II B; consequently, $R = 5$ a.u., $\theta \simeq 100°$, $\phi = 0°$, and $\phi' = \theta' = 90°$. Let us consider this on some examples below.

The first three contour plots [Figs. 6(a)–6(c)] describe the radial dependence of the PES as a function of different angular parameters (θ, ϕ, and ϕ', respectively). As one can see, the radial dependence is very strong and rather isotropic. In the plot of θ vs R [Fig. 6(a)], one can observe a single, deep minimum around 102°. The well around the minimum is narrow and sharp. The PES here changes quickly, especially with respect to R. Except in the well region, large anisotropies could not be found; however, the PES is quite asymmetric with respect to θ.

The radial dependence as a function of ϕ angle is somewhat stronger [see Fig. 6(b)]. The deepest minimum is located at 0° here,

and two additional minima can be observed around ±145°. The PES is characterized by perfect bilateral (left–right) symmetry with respect to ϕ. The well regions are wider and are not so sharp, as in the case of the previous contour plot. The radial anisotropy is significant only below $R \sim 8$ bohrs.

In order to characterize the radial dependence of the PES with respect to ϕ', it is enough to consider a smaller angular interval from 0° to 180°. The features of the PES periodically repeated after every 180° rotation. As shown in Fig. 6(c), only one deep minimum is observed in this slice of the PES at $\phi' = 90°$ (or $\phi' = -90°$). The size and the shape of the well is rather similar to that observed in the case of θ vs R dependence. However, in this case, a perfect left–right symmetry is observed in the ϕ'-dependence with respect to 90° at the minimum.

We also analyzed the dependence of the PES on different angular coordinates simultaneously at a fixed intermolecular distance of $R = 5$ bohrs. Figures 6(d) and 6(e) show the PES contours with respect to θ as functions of ϕ and ϕ' coordinates, respectively. As one can see, the anisotropy of the PES is much stronger than that observed in the previous cases. It is also highly asymmetric in the two contour plots. While the potential changes intensively with respect to θ at any ϕ, ϕ' values, we observe only slight changes with respect to both ϕ and ϕ' at those θ angles, which are far from the position of the minimum (i.e., at $\theta \to 0°$ and $\theta \to 180°$). In the numerical analysis of the PES, we found that both the ϕ-dependenc and ϕ'-dependence show a perfect left–right symmetry with respect to 0°, which could be observed also in Figs. 6(b) and 6(c). This is due to the features of our coordinate system: one hydrogen atom of the H_3O^+ cation lies in the *xz*-plane (i.e., in the $\phi = 0°$ direction, see Fig. 1). It is worth noting, however, that the anisotropic angular interval in the case of ϕ is twice as large (180°), compared to the case of ϕ' (90°). As one can see, the PES also shows a slight spherical symmetry in terms of θ vs ϕ', but only in the potential well region.

Finally, we describe the θ'-dependence as functions of θ and ϕ spherical angles in Figs. 6(f) and 6(g). As one can see, the anisotropy
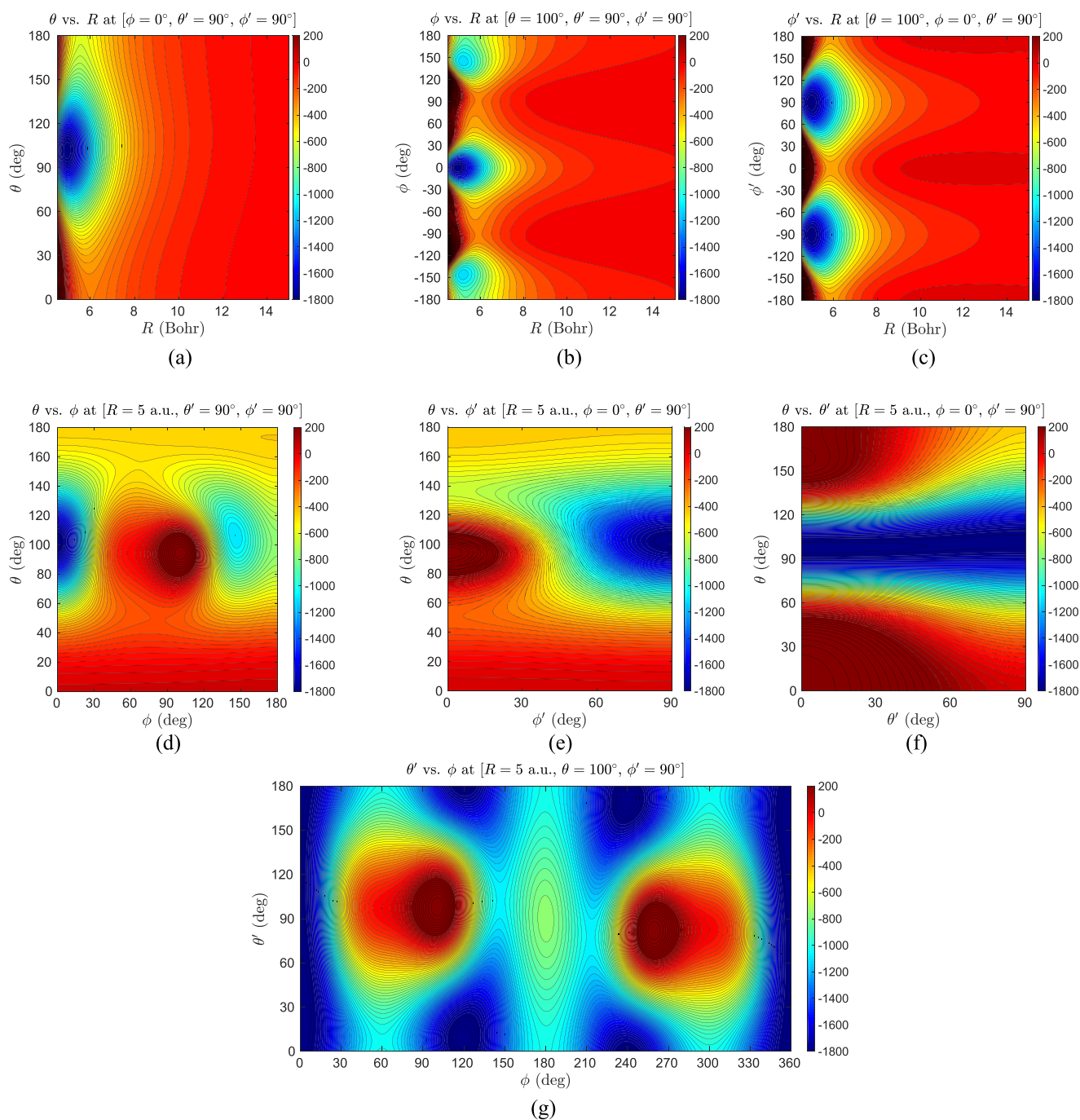
FIG. 6. Contour plots showing the dependence of the PES from the radial and angular parameters: (a) θ vs R, (b) ϕ vs R, (c) ϕ' vs R, (d) θ vs ϕ, (e) θ vs ϕ', (f) θ vs θ', and (g) θ' vs ϕ.

of the PES is even stronger, compared to the previous cases, especially in the θ' vs ϕ contour plot. In this plot, one can observe a very asymmetric PES for which it is not likely to find any reference point or axis to define higher symmetric behavior. At the same time,

according to our numerical analysis, the dependence of θ vs θ' also shows a perfect left–right symmetry with respect to the θ' coordinate with turning point at 90°. This symmetric behavior is related to the identical hydrogen atoms of the H_2 molecule, which could be

"exchanged" in every 90° rotation of the molecule. It is also worth noting that the dependence of the PES on this angular parameter is rather small, in general. For example, the deepness of the potential well for $\theta = 80°$–$110°$ is almost not affected by the change in θ' coordinate. A similar behavior is observed in the case of the PES contour in Fig. 6(g). In the region of the well around $\phi = 0°$ and the barrier around $\phi = 180°$, the PES does not depend strongly on the θ' parameter. However, in the region of $\phi = 100°$–$120°$, both deep potential wells (around $\theta' = 10°$ and $\theta' = 180°$) and a high barrier (around $\theta' = 100°$) can be observed. Similar tendencies were observed in this PES at $\phi = 240°$–$260°$ spherical angles, but at other θ' values.

As one can see from the above analysis, the overall angular anisotropy of the PES is rather strong. It is worth noting, however, that the potential well is well-defined and narrow. As we mentioned earlier, in some angular coordinates, a quite large left–right symmetry can be observed, which reduces the complexity of the PES, in general. This left–right symmetry was explicitly shown only for the radial dependencies in Figs. 6(b) and 6(c).

C. Results of bound-state calculations

We calculated the bound rotational levels based on the new PES for all nuclear spin species of the interaction system: o-H_3O^+–o-H_2, o-H_3O^+–p-H_2, p-H_3O^+–o-H_2, and p-H_3O^+–p-H_2. A good convergence was achieved in terms of the rotational basis size for all nuclear-spin species with $J_{tot} = 0, 1$, except for p-H_3O^+–o-H_2, where memory requirements exceeded the available resources. In the case of the latter, the number of rotational levels to be involved in the calculations for a good convergence is more than 1900, while the total number of Gaussian basis functions exceeds 100 000. It should be noted that in order to save CPU time/memory, from the full 208-term fit, a subset of 55 angular basis functions (including all anisotropies up to $l_1 = 6$ and $l_2 = 2$) was selected as the optimal expansion for dynamical calculations.

While constructing the set of rotational basis functions [see Eq. (6)], our radial grid covered the range from $R_{min} = 4.5$ a.u. up to $R_{max} = 27$ a.u. with a constant of 0.35 a.u. distance between the centers of the Gaussian functions. For the α exponential scaling factor, the 6.32 value was found to be suitable. The bound rotational states of the collisional system were computed then from the constructed basis functions. For the integration, we used a rather dense uniform grid with 0.02 a.u. step size in the whole range of the R-space.

From the bound-state eigenvalues, we computed the D_0 dissociation energies for all nuclear spin species according to Eq. (7). The reference values are the internal energies of the ground rotational levels of the H_3O^+–H_2 complex with the corresponding symmetry, i.e., E_0^{int} for the $j_k^\varepsilon = 1_0^+$ state involving o-H_3O^+ and the $j_k^\varepsilon = 1_1^+$ state in the case of p-H_3O^+. The results for dissociation energies along with the corresponding ground-level internal energies and total angular momenta are listed in Table II. We found that the o-H_3O^+–p-H_2 and p-H_3O^+–o-H_2 dimers have a ground-state with $J_{tot} = 1$, while in the two other nuclear-spin configurations, the dimers have a ground-state with $J_{tot} = 0$. These observations are in accordance with the bound-state data of Surin et al.[41] for the o-NH_3–o-H_2 and p-NH_3–o-H_2 spin species. The calculated D_0 values are rather large, which can be related to the deep well of the interaction potential (~ 1887 cm^{-1}). As one can see, D_0 is considerably larger (by more than 59 cm^{-1}) for the H_3O^+–ortho-H_2 complexes than for the H_3O^+–para-H_2

TABLE II. Calculated D_0 dissociation energies with the corresponding E_0^{int} ground-level internal energies and J_{tot} total angular momenta for the H_3O^+–H_2 nuclear-spin species.

Nuclear-spin species	D_0 (cm^{-1})	J_{tot}	E_0^{int} (cm^{-1})
ortho-H_3O^+–ortho-H_2	1124.497	0	141.069
ortho-H_3O^+–para-H_2	1065.053	1	22.309
para-H_3O^+–ortho-H_2	1108.228	1	136.106
para-H_3O^+–para-H_2	1042.779	0	17.364

systems, since the H_2 rotational wavefunction can polarize to sample the most attractive geometry of the complex.[42] Similar tendencies were observed for the lowest bound states of other molecule-H_2 complexes for which the dissociation energies are significantly larger in the case of ortho-H_2 than for para-H_2 (see, for example, Refs. 39 and 41–43). We found a few hundred bound states for all nuclear spin configurations. For the states with $J_{tot} = 1$, more states can be associated with the complexes involving ortho-H_2 than those of involving para-H_2. This is especially remarkable when the interacting partner is para-H_3O^+. These observations are also in agreement with the findings of the previously cited works.

IV. CONCLUSIONS

We have presented in this work a five-dimensional rigid-rotor PES to study the collision of hydronium cation and molecular hydrogen. The calculations were performed using the explicitly correlated CCSD(T)-F12 coupled-cluster theory along with the standard aug-cc-pVTZ basis set. The ab initio potential energy surface, which consists of 99 000 points, was fitted over a set of analytical angular functions in order to effectively use it for collisional dynamics studies. While the angular anisotropy of the potential is rather large, the final expansion contains 208 basis function terms. The rms residual of the fit is below 1 cm^{-1} in the minimum and long-range region of the PES.

We have also analyzed the possible reactive processes that can be relevant in H_3O^+–H_2 collisions. The enthalpy change and the interaction energy for the possible chemical reaction channels were calculated. We found that the system under study is a van der Waals complex, which has a chemically non-reactive nature. We did not find any transition states along the collision pathway of the system. Based on the analysis, we can conclude that the hydrogen exchange process and those chemical reactions, which correspond to the formation of new molecular species, are not likely to occur and can be neglected.

We have calculated the lowest singlet and triplet excited electronic states of the H_3O^+–H_2 system along a one-dimensional radial cut of the potential. All of these states are far from the ground electronic state, and so the collision complex does not have a strong multiconfigurational nature, and the interaction potential can be adequately calculated by single-reference ab initio methods. This is also supported by the results of T_1 and D_1 diagnostics, which was provided to benchmark the CCSD(T)-F12 calculations along the RC.

We have focused in the current study on providing an angular expansion for the H_3O^+–H_2 potential energy surface, which can be suitable for close-coupling dynamical calculations. It should be noted, however, as follows:

- The well depth of the analytical potential energy surface is rather large, about 1887.2 cm^{-1}. The scattering studies of the system will involve many rotational levels, as also found from the results of our bound-state calculations.
- The D_0 dissociation energies are large for all possible *ortho*- and *para*-nuclear spin species. In the case of *ortho*-H_2, the value of D_0 is somewhat larger: about 1108 cm^{-1} and 1124 cm^{-1} when interacting with *para*- and *ortho*-H_3O^+, respectively.
- For the same interacting systems involving *para*-H_2, the dissociation energies are somewhat lower, but still rather large (about 1043 cm^{-1} and 1065 cm^{-1}, respectively).
- The difference between the two H_2 nuclear spin isomers is in accordance with the results of the previous studies, where the interaction of molecular hydrogen with other molecular and ionic species was investigated.

The recently developed, advanced *ab initio* methods allow one to treat the many-dimensional interaction potential of large molecular systems with high accuracy. We should emphasize that the explicitly correlated CCSD(T)-F12 theory is probably the best single-reference approach, which can be effectively used to calibrate the intermolecular PES of these collisional systems at the wavenumber level of accuracy. Because the system under study has a non-reactive, single-configuration nature, for which the coupled-cluster theory performs very well and rarely fails, the findings of the present work can be used confidently for further dynamical studies successfully.

SUPPLEMENTARY MATERIAL

See the supplementary material for the *ab initio* datasets, the expansion coefficients of the PES, and the FORTRAN routines corresponding to construct the fitted potential.

ACKNOWLEDGMENTS

DATA AVAILABILITY

The data that support the findings of this study are available within the article and its supplementary material.

REFERENCES

[1] T. G. Phillips, E. F. van Dishoeck, and J. Keene, Astrophys. J. **399**, 533 (1992).

[2] E. González-Alfonso, J. Fischer, S. Bruderer, H. S. P. Müller, J. Graciá-Carpio, E. Sturm, D. Lutz, A. Poglitsch, H. Feuchtgruber, S. Veilleux, A. Contursi, A. Sternberg, S. Hailey-Dunsheath, A. Verma, N. Christopher, R. Davies, R. Genzel, and L. Tacconi, Astron. Astrophys. **550**, A25 (2013); arXiv:1211.5064 [astro-ph.GA].

[3] A. R. Offer and M. C. van Hemert, Chem. Phys. **163**, 83–89 (1992).

[4] D. Hollenbach, M. J. Kaufman, D. Neufeld, M. Wolfire, and J. R. Goicoechea, Astrophys. J. **754**, 105 (2012).

[5] F. F. S. van der Tak, S. Aalto, and R. Meijerink, Astron. Astrophys. **477**, L5–L8 (2008).

[6] J. R. Goicoechea and J. Cernicharo, Astrophys. J. **554**, L213–L216 (2001).

[7] M. Gerin, M. De Luca, J. Black, J. R. Goicoechea, E. Herbst, D. A. Neufeld, E. Falgarone, B. Godard, J. C. Pearson, D. C. Lis, T. G. Phillips, T. A. Bell, P. Sonnentrucker, F. Boulanger, J. Cernicharo, A. Coutens, E. Dartois, P. Encrenaz, T. Giesen, P. F. Goldsmith, H. Gupta, C. Gry, P. Hennebelle, P. Hily-Blant, C. Joblin, M. Kazmierczak, R. Kolos, J. Krelowski, J. Martin-Pintado, R. Monje, B. Mookerjea, M. Perault, C. Persson, R. Plume, P. B. Rimmer, M. Salez, M. Schmidt, J. Stutzki, D. Teyssier, C. Vastel, S. Yu, A. Contursi, K. Menten, T. Geballe, S. Schlemmer, R. Shipman, A. G. Tielens, S. Philipp-May, A. Cros, J. Zmuidzinas, L. A. Samoska, K. Klein, and A. Lorenzani, Astron. Astrophys. **518**, L110 (2010).

[8] E. Herbst and W. Klemperer, Astrophys. J. **185**, 505–533 (1973).

[9] A. Sternberg and A. Dalgarno, Astrophys. J., Suppl. Ser. **99**, 565 (1995); http://articles.adsabs.harvard.edu/pdf/1995ApJS...99..565S.

[10] L. Vejby-Christensen, L. H. Andersen, O. Heber, D. Kella, H. B. Pedersen, H. T. Schmidt, and D. Zajfman, Astrophys. J. **483**, 531–540 (1997).

[11] M. J. Jensen, R. C. Bilodeau, C. P. Safvan, K. Seiersen, L. H. Andersen, H. B. Pedersen, and O. Heber, Astrophys. J. **543**, 764–774 (2000).

[12] V. Zhaunerchyk, W. D. Geppert, S. Rosén, E. Vigren, M. Hamberg, M. Kamińska, I. Kashperka, M. Af Ugglas, J. Semaniak, M. Larsson, and R. D. Thomas, J. Chem. Phys. **130**, 214302 (2009).

[13] S. Yu, B. J. Drouin, J. C. Pearson, and H. M. Pickett, Astrophys. J., Suppl. Ser. **180**, 119–124 (2009).

[14] Q. Yu and J. M. Bowman, J. Chem. Theory Comput. **12**, 5284–5292 (2016).

[15] J. E. Mann, Z. Xie, J. D. Savee, J. M. Bowman, and R. E. Continetti, J. Phys. Chem. A **117**, 7256–7266 (2013).

[16] C. Domesle, S. Dziarzhytski, N. Guerassimova, L. S. Harbo, O. Heber, L. Lammich, B. Jordon-Thaden, A. Wolf, and H. B. Pedersen, Phys. Rev. A **88**, 043405 (2013).

[17] H. B. Pedersen, S. Altevogt, B. Jordon-Thaden, O. Heber, L. Lammich, M. L. Rappaport, D. Schwalm, J. Ullrich, D. Zajfman, R. Treusch, N. Guerassimova, M. Martins, and A. Wolf, Phys. Rev. A **80**, 012707 (2009).

[18] V. Špirko and W. P. Kraemer, J. Mol. Spectrosc. **134**, 72–81 (1989).

[19] X. Huang, S. Carter, and J. M. Bowman, J. Phys. Chem. B **106**, 8182–8188 (2002).

[20] A. Neau, A. Al Khalili, S. Rosén, A. Le Padellec, A. M. Derkatch, W. Shi, L. Vikor, M. Larsson, J. Semaniak, R. Thomas, M. B. Någård, K. Andersson, H. Danared, and M. Af Ugglas, J. Chem. Phys. **113**, 1762–1770 (2000).

[21] H. El Hanini, F. Najar, M. Naouai, and N.-E. Jaidane, Phys. Chem. Chem. Phys. **21**, 11705–11713 (2019).

[22] *Gas-Phase Chemistry in Space*, edited by F. Lique and A. Faure (IOP Publishing, 2019), pp. 2514–3433.

[23] A. Faure and J. Tennyson, Mon. Not. R. Astron. Soc. **340**, 468–472 (2003).

[24] S. F. Boys and F. Bernardi, Mol. Phys. **19**, 553–566 (1970).

[25] N. Bouhafs, C. Rist, F. Daniel, F. Dumouchel, F. Lique, L. Wiesenfeld, and A. Faure, Mon. Not. R. Astron. Soc. **470**, 2204–2211 (2017); arXiv:1706.00732.

[26] E. Roueff and F. Lique, Chem. Rev. **113**, 8906–8938 (2013); arXiv:1310.8259.

[27] S. Green, J. Chem. Phys. **73**, 2740–2750 (1980).

[28] S. Maret, A. Faure, E. Scifoni, and L. Wiesenfeld, Mon. Not. R. Astron. Soc. **399**, 425–431 (2009).

[29] P. Valiron, M. Wernli, A. Faure, L. Wiesenfeld, C. Rist, S. Kedžuch, and J. Noga, J. Chem. Phys. **129**, 134306 (2008).

[30]S. Bubin and L. Adamowicz, J. Chem. Phys. **118**, 3079–3082 (2003).

[31]J. Tang and T. Oka, J. Mol. Spectrosc. **196**, 120–130 (1999).

[32]H.-J. Werner, P. J. Knowles, G. Knizia, F. R. Manby, M. Schütz *et al.*, Molpro, version 2015.1, a package of *ab initio* programs, 2015.

[33]H.-J. Werner, P. J. Knowles, G. Knizia, F. R. Manby, and M. Schütz, Wiley Interdiscip. Rev.: Comput. Mol. Sci. **2**, 242–253 (2012).

[34]M. J. Frisch, G. W. Trucks, H. B. Schlegel, G. E. Scuseria, M. A. Robb *et al.*, Gaussian 09, Revision E.1, Gaussian, Inc.Wallingford, CT, 2009.

[35]K. A. Peterson, D. E. Woon, and T. H. Dunning, J. Chem. Phys. **100**, 7410–7415 (1994).

[36]M. H. Alexander, D. E. Manolopoulos, H.-J. Werner, B. Follmeg, P. F. Vohralik, with contributions by D. Lemoine, G. Corey, T. Johnson, B. Orlikowski, A. Berning, A. Degli-Esposti, C. Rist, P. Dagdigian, B. Pouilly, G. van der Sanden, M. Yang, F. de Weerd, S. Gregurick, J. Klos, and F. Lique, HIBRIDON is a package of programs for the time-independent quantum treatment of inelastic collisions and photodissociation.

[37]C. Rist, M. H. Alexander, and P. Valiron, J. Chem. Phys. **98**, 4662–4671 (1993).

[38]C. Rist and A. Faure, J. Math. Chem. **50**, 588–601 (2012).

[39]Q. Ma, J. Kłos, M. H. Alexander, A. van der Avoird, and P. J. Dagdigian, J. Chem. Phys. **141**, 174309 (2014).

[40]I. P. Hamilton and J. C. Light, J. Chem. Phys. **84**, 306–317 (1986).

[41]L. A. Surin, I. V. Tarabukin, S. Schlemmer, A. A. Breier, T. F. Giesen, M. C. McCarthy, and A. v. d. Avoird, Astrophys. J. **838**, 27 (2017).

[42]Q. Ma, A. van der Avoird, J. Loreau, M. H. Alexander, S. Y. Van De Meerakker, and P. J. Dagdigian, J. Chem. Phys. **143**, 044312 (2015).

[43]J. Kłos, Q. Ma, M. H. Alexander, and P. J. Dagdigian, J. Chem. Phys. **146**, 114301 (2017).

[44]K. P. Huber and G. Herzberg, "Constants of diatomic molecules," in *Molecular Spectra and Molecular Structure* (Springer US, Boston, MA, 1979), pp. 8–689.

[45]D. Smith and N. G. Adams, Astrophys. J. **217**, 741–748 (1977).

[46]S. W. Englander, N. W. Downer, and H. Teitelbaum, Annu. Rev. Biochem. **41**, 903–924 (1972).

[47]J. K. Kim, L. P. Theard, and W. T. Huntress, Jr., J. Chem. Phys. **62**, 45–52 (1975).

[48]T. J. Lee and P. R. Taylor, Int. J. Quantum Chem. **36**, 199–207 (1989).

[49]W. Jiang, N. J. Deyonker, and A. K. Wilson, J. Chem. Theory Comput. **8**, 460–468 (2012).

[50]T. J. Lee, Chem. Phys. Lett. **372**, 362–367 (2003).

[51]T. R. Phillips, S. Maluendes, A. D. McLean, and S. Green, J. Chem. Phys. **101**, 5824–5830 (1994).